Eur. J. Mineral.
2011, **23**, 157–168
Published online February 2011

Melting textures and microdiamonds preserved in graphite pseudomorphs from the Beni Bousera peridotite massif, Morocco

FATIMA EL ATRASSI[1], FABRICE BRUNET[1,*], MOHAMED BOUYBAOUENE[2], CHRISTIAN CHOPIN[1] and GILLES CHAZOT[3,4]

[1] Laboratoire de Géologie, Ecole normale supérieure – CNRS, 24 rue Lhomond, 75005 Paris, France
*Corresponding author, e-mail: fabrice.brunet@obs.ujf-grenoble.fr
[2] Laboratoire d'océanologie, géodynamique et génie géologique, Université Mohammed V, avenue Ibn Battouta, B.P. 1014, Rabat, Morocco
[3] Université Européenne de Bretagne, Brest, France
[4] Université de Brest, CNRS, UMR 6538 Domaines Océaniques, Place Copernic, 29280 Plouzané, France

Abstract: Over 30 graphite aggregates that represent pseudomorphs after diamond were manually extracted from a garnet pyroxenite layer in the Beni Bousera peridotite massif, northern Morocco. The inclusions present in the aggregates were characterized by combining scanning electron microscopy, micro-Raman spectroscopy and cathodoluminescence. Large composite clinopyroxene–orthopyroxene–garnet inclusions (*ca*. 500 μm across) are common in the core of the graphite aggregates. Silicate films with a thickness of a few micrometres occur intercalated between graphite flakes throughout each aggregate. They are of basaltic composition and are interpreted as partial melts formed by *in situ* melting of the large composite inclusions and, possibly, of the host pyroxenite, during the Beni Bousera massif uplift. In addition, various solid inclusions composed of chlorides, sulphates and carbonates are found to be evenly distributed irrespective of the graphite aggregate texture (coarse in the core, in some instances fine-grained on the rim). Diamond crystals, 0.5–2 μm in size, were also observed in several aggregates, apparently included in large graphite flakes, and were characterized using cathodoluminescence and Raman micro-spectroscopies. They are interpreted as relics of large mantle-stage diamonds, now heavily graphitized. This finding confirms earlier propositions that the graphite aggregates in Beni Bousera and Ronda garnet pyroxenites are pseudomorphs after diamond and raises questions on the kinetics of graphitization.

Key-words: graphite, diamond, orogenic peridotite, garnet pyroxenite, Beni Bousera, silicate melt films, partial melting, cathodoluminescence, Raman spectroscopy.

1. Introduction

Orogenic peridotite massifs represent large and continuous pieces of the Earth's upper mantle that are exposed in mountain belts. Consequently, they are unique objects for the study of relatively large-scale processes affecting the upper mantle. However, these upper-mantle bodies have undergone, prior to their present exposure as orogenic massifs, a series of events such as decompression, cooling, partial melting, exhumation, etc, that have modified their original physical and chemical characteristics. These events may be recorded by specific mineral assemblages and textures like, *e.g.* majoritic garnet and diamond for the highest-pressure stages, melt inclusions, pseudomorphs, exsolution features during cooling and decompression. Therefore, finding and interpreting relics of such assemblages and textures has been a major petrological and geochemical goal over the last decades, during which the ever increasing spatial resolution of observation and analytical tools has allowed ever tinier pieces of evidence to be examined. Microdiamond findings in peridotite bodies of the Caledonian Western Gneiss Region of Norway and the associated radiometric ages are a good illustration of how microscale observation and analysis can reveal a complex and multistage history, which can be traced back into the Archean (*e.g.*, the review of van Roermund, 2009).

Centimetre-sized graphite aggregates in garnet-pyroxenite layers of the Beni Bousera peridotite massif (BB) in northern Morocco and the Ronda peridotite massif in the Betic Cordilleras (southern Spain) have been interpreted as pseudomorphs after diamond on the basis of morphological arguments (Slodkevich, 1980; Pearson *et al*., 1989; Davies *et al*., 1993). The original nature of the pseudomorphs makes these rocks by far the most diamond-rich known on Earth – at some early stage of their evolution (Pearson *et al*., 1989). In an attempt at reconstructing this early evolution, we have undertaken a detailed

DOI: 10.1127/0935-1221/2011/0023-2094
0935-1221/11/0023-2094 $ 5.40

investigation of the graphite aggregates and enclosing garnet-pyroxenite in the BB massif. We report here on the nature of micro-inclusions found in the graphite aggregates, which establishes the presence of diamond and brings textural evidence for partial melting.

2. Geological setting

The Beni Bousera and the Ronda peridotite massifs are located in the western termination of the Alpine Mediterranean orogen (*i.e.,* convergence between the African and Eurasian plates). Studies of these massifs have revealed a protracted and polyphased history with, possibly, a first undated phase of ascent from 140 to 200 km (diamond stability field) to shallower levels (around 70 km, in the spinel-peridotite facies) and a second phase of extensional emplacement within the nappe pile of the Betic-Rif orogen, at mid-crustal levels, accompanied by heating and partial melting (*e.g.*, Van der Wal & Vissers, 1993; Lenoir *et al*., 2001). The mechanisms responsible for this later phase, in particular the respective role of mantle diapirism (*e.g.*, Loomis, 1975; Tubia & Cuevas, 1986), lithospheric delamination (*e.g.*, Platt & Vissers, 1989; Platt *et al*., 2003a), slab detachment (*e.g.*, Zeck, 1996, 1997), slivering and exhumation in a subduction-collision context (*e.g.*, Chalouan & Michard, 2004 and references therein) and slab retreat (*e.g.*, Jolivet *et al*., 2008), are still matter of debate.

Whatever the lithospheric-scale scenario, a robust constraint on the early history of these two orogenic massifs is the presence of large and abundant graphite aggregates within carbon-rich garnet-pyroxenite layers, interpreted as pseudomorphs after diamond (Slodkevich, 1980; Pearson *et al*., 1989; Davies *et al*., 1993). These garnet pyroxenites crystallized in the host peridotite massif about 1.2–1.4 Ga ago (Reisberg *et al*., 1991; Kumar *et al*., 1996) and originate from depths of, at least, 140 km. According to garnet – clinopyroxene thermometry, high temperatures in the order of 1300 °C were then experienced by these garnet pyroxenites at pressures within the graphite field (Kornprobst *et al*., 1990). Original diamonds would have transformed into graphite aggregates, which then witnessed the entire history of the host garnet pyroxenites until their exhumation by tectonic thinning about 20–25 Ma ago (Negro *et al*., 2006 and references therein).

3. Previous studies

The graphite aggregates are found in garnet pyroxenite layers where they form up to 15 % of the rock volume (Pearson *et al*., 1989). Some show an octahedral morphology; this unusual habit for graphite was interpreted as a pseudomorphic replacement after a mineral of cubic symmetry with the basal (001) planes of graphite being parallel to the {111} faces of the cubic-symmetry mineral precursor (Slodkevich, 1980; Pearson *et al*., 1989). Several lines of evidence converge which indicate that diamond rather than, for example, spinel-group minerals was precursor for the graphite pseudomorphs:

(1) the isochemical nature of the diamond – graphite transformation and the absence of spinel relics within the graphite aggregates (Pearson *et al*., 1989);
(2) the cubo-octahedral faceting of clinopyroxene inclusions with the {100} and {111} faces of both inclusion and host octahedral graphite aggregate being parallel (Slodkevich, 1980; Pearson *et al*., 1989);
(3) the occurrence of textural heterogeneity within some graphite aggregates, with cores made of coarse and regular graphite flakes, surrounded by radial and perpendicular graphite planes of smaller size (Slodkevich, 1980, see also Fig. 1a in Pearson *et al*., 1991, and Fig. 13.5 in Pearson *et al*., 1995, ''coat graphite''); this type of texture has been interpreted as inherited from ''coated diamond'' precursors (Pearson *et al*., 1989, 1991);
(4) the apparent crystallographic relationship between graphite flakes orientation and former diamond faces (Pearson *et al*., 1989).

Finally, the $\delta^{13}C$ isotopic composition of the graphite aggregates in both massifs (–16 to –27.6 per mil with a mode around –21 per mil in Beni Bousera, Pearson *et al*., 1991) suggests that the alleged precursor diamond crystallized from a ^{13}C depleted source, possibly from subducted crust. Apart from garnet and pyroxene (interpreted as inclusions of minerals of the host pyroxenite, Pearson *et al*., 1989), the nature of the phases trapped in the Beni Bousera or Ronda graphite aggregates has received little attention so far, in spite of the abundant dataset on mineral and fluid inclusions in natural diamonds from various settings and the geodynamical information that these inclusions can potentially hold.

4. Sample preparation and analytical techniques

A set of graphite aggregates was extracted from the graphite–garnet-pyroxenite (GGP) mafic layer outcropping in the streambed of Oued el Jouj (called Oued Tasemourt on Fig. 1 of Kornprobst *et al*., 1990, which locates the GGP), in the south-western Beni Bousera massif. The conventional procedure which consists in cutting and polishing the sample for characterization could not be followed here because of the remarkable softness of the graphite aggregates [and of our wish to avoid any diamond-bearing preparation tool or material]. Tiny inclusions in the graphite aggregate would be removed, and even the microstructure of graphitic materials can be modified by polishing (*e.g.*, Pasteris, 1989; Mostefaoui *et al*., 2000); in addition, contamination from host-rock or grinding/polishing material would be difficult to avoid. Therefore, the graphite aggregates studied here were extracted manually from the host-rock pyroxenite for characterization. Large graphitic garnet pyroxenite blocks were

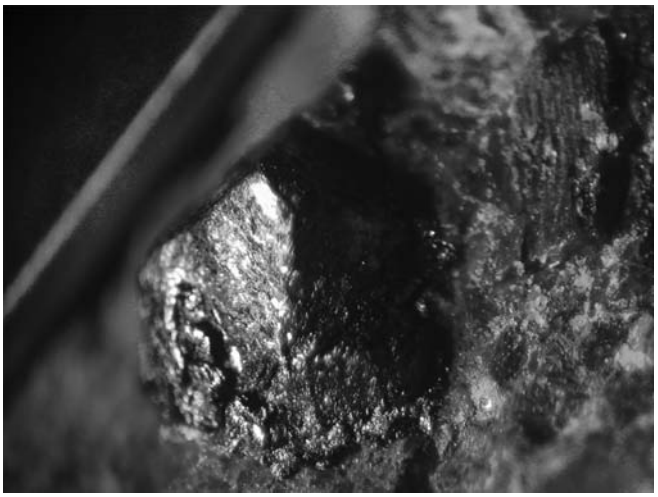

Fig. 1. Photograph of a cubo-octahedral graphite aggregate (*ca.* 1 mm across) still attached to the host garnet pyroxenite and displaying {111} faces (four-fold axis piercing toward the upper left).

crushed into pieces down to 5–10 cm size, which were then split with a hammer. When a piece of graphite aggregate was visible on a fresh section, it was carefully extracted from the host rock using a metal needle. Between 30 and 40 graphitic specimens, 2–5 mm in size, were extracted according to this procedure. It must be noted that part of the outer shell of the aggregates might have been lost since it could have remained stuck to neighbouring minerals in the host rock.

Extracted graphite aggregates were glued with conductive carbon cement onto a metal holder for further scanning electron microscope (SEM) characterization, in such a way that the fresh irregular fracture surface of the specimen was exposed to the electron beam. One of the samples which displayed large silicate inclusions was gold-palladium coated for scanning electron microscope (SEM) imaging and qualitative analysis by energy-dispersive spectrometry (EDS) using a Zeiss Σigma™ field-emission-gun SEM (FE-SEM) equipped with a large-area (50 mm^2) EDS silicon drift detector, X-Max Oxford Instruments, at ENS (Paris). The other aggregates were observed directly without coating in order to avoid contamination and, eventually, to allow further cathodoluminescence study (ZEISS SUPRA 55 VP SEM equipped with a Jobin-Yvon Horiba SAS cathodoluminescence acquisition OPEA system at Université P. et M. Curie, Paris) and Raman microspectroscopy investigation. For the latter, the Renishaw inVia spectrometer at ENS was used, either with a 514.5 nm argon laser or with a 785 nm diode laser, focussed through a DMLM Leica microscope with a × 100 objective of 0.85 numerical aperture. The signal was filtered by edge filters, dispersed by a 1200 or 1800 grooves/mm grating and analysed with a Peltier cooled RENCAM CCD detector. Before each session the spectrometer was calibrated against an Si standard and the wavenumber calibration was checked regularly. Spectra were treated using the program PeakFit 3.0 (Jandel Scientific) and Raman bands fitted with a Voigt profile.

Four grains (graphite aggregates) were ground together, in an agate mortar, down to a fine powder for X-ray diffraction (Rigaku UltraX18HF, Cu rotating anode, beam conditions: 40 kV, 300 mA). Three other grains were gently ground for SEM inspection; the obtained powder was dispersed on a double-sided carbon tape.

For a comparative micro-Raman spectroscopic study with the microdiamonds found in the graphite aggregates, the 1-μm diamond polishing paste (Scandia® M-type) and spray (Mecaprex®) used in the laboratory by other workers were smeared on an aluminium holder and washed with ethanol. The diamond grains remaining implanted on the metal were characterized using the same instrument (785 nm Renishaw diode laser) under the same analytical conditions as for the natural samples.

5. Results

5.1. Morphology, petrography and texture of the graphite aggregates

The original morphology of the graphite aggregates is difficult to assess from the sections that are obtained by splitting the sample. However, in a few instances, euhedral cubo-octahedral morphology could be observed (Fig. 1) in agreement with earlier observations (Slodkevich, 1980; Pearson *et al.*, 1989). It appears that, in most instances, the graphite aggregates had been split by the extraction procedure along large graphite flakes (around 500 μm across) which are therefore well-exposed on the SEM images (Fig. 2a). These large flakes may either extend up to the outer surface of the aggregate (Fig. 2c) or they can end on a rim composed of graphite grains with a different orientation and with shorter extension for the graphene planes (10–50 μm, Fig. 2b). The apices of cubo-octahedral aggregates are found to be composed of such smaller graphite grains (Fig. 2a).

Raman micro-spectrometry on the graphite aggregates confirms the structural difference observed by SEM between rim and core graphite in some aggregates. Large flakes that compose most of the specimen display Raman spectra of perfectly ordered graphite with no measurable defect band. In contrast, smaller graphite flakes found towards the specimen rim show, in some instances, defect bands (D1 and D2) centred around 1358 and 1622 cm^{-1}, respectively (Fig. 3). The diffraction pattern collected on the ground specimen confirms the high level of crystallinity already pointed out by the micro-Raman data, with a FWHM of 0.144 (2θ) for the graphite basal reflexion, sharper than that measured on reference Sri Lanka natural graphite (Erdosh, 1970; Balasooriya *et al.*, 2007) under the same analytical vconditions ($\Delta 2\theta = 0.179$).

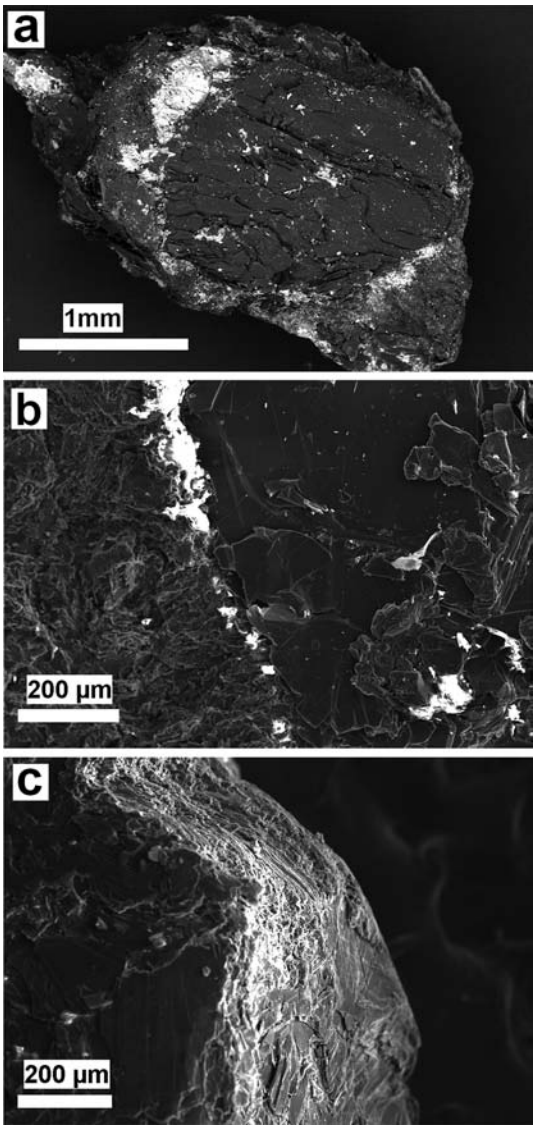

Fig. 2. FE-SEM images (BSE mode, no coating) of graphite pseudomorphs extracted from the garnet pyroxenite host-rock and broken manually with a metal needle into two pieces. (a) Large graphite flakes (>500 µm across) exposed in the centre of the aggregate. Note that the large-flakes zone is rimmed by insulating silicate matter. The bottom right apex of the aggregate is composed of smaller graphite grains (<100 µm). (b) Contact between large graphite flakes (core) and the outer rim of the aggregate made of graphite grains with shorter graphene planes (10–50 µm). Note that the contact is rimmed by intercalated silicate-rich matter (electrical insulator). (c) Large graphite flakes (>500 µm across) extending up to the outer surface of the sampled aggregate.

The interior of the aggregates is ubiquitously rich in large areas of a thin insulating material, as evidenced by charge accumulation (Fig. 2a, c and 4). This type of very fine and delicate feature would be unlikely to survive cutting or polishing. Qualitative analyses (EDS data on unpolished material) indicate that this insulating material is composed of silicate matter (Fig. 4).

Large polymineralic inclusions with sizes of up to several hundred micrometres are ubiquitous in the core of the graphite aggregates, as observed on cut hand samples and on

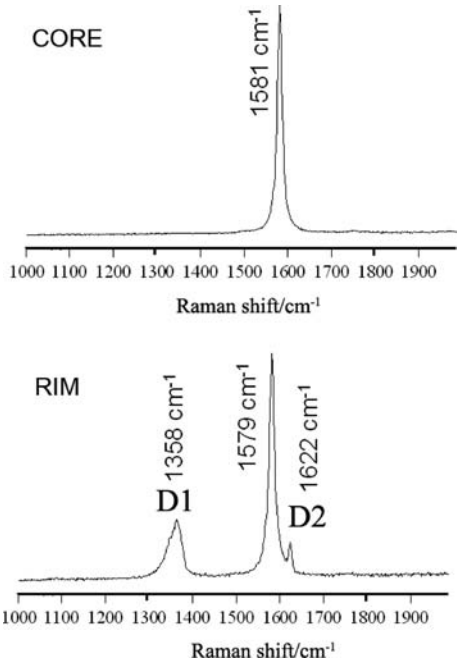

Fig. 3. Micro-Raman spectra collected on the core (large flakes, *ca.* 500 µm) and on the rim (shorter flakes, 10–50 µm) of a graphite aggregate.

thin sections. This type of macro-inclusion has been found in the section of one of the hand-extracted graphite aggregate. Elemental X-ray mapping (after gold-palladium coating) revealed a clinopyroxene crystal containing thick orthopyroxene exsolution lamellae (Fig. 5). This type of cooling texture is also visible in the host rock (*e.g.*, Kornprobst, 1969). The striped clinopyroxene inclusion is rimmed by small garnet grains which are, themselves, surrounded by plagioclase/orthopyroxene/spinel intergrowths (Fig. 5).

5.2. Intercalated silicate film inclusions

The thin silicate films (at most 1–5 µm thickness) described above as a ubiquitous feature in all the graphite aggregates (in both large central flakes and polycrystalline rims) clearly appear to be intercalated, at various scales, within stacks of (001) graphene planes (Fig. 3), suggesting either co-crystallization with graphite or percolation along graphite planes. The textural relationship between silicate films and a composite macro-inclusion made of cpx-opx-garnet is illustrated in Fig. 5: the outer rim of the entire inclusion appears to be in physical continuity with the thin silicate film. A set of semi-quantitative analyses collected on the silicate films from various specimens (Fig. 6) indicate a composition ranging from picro-basalt to basaltic andesite, with a silica content around 45–50 wt% (Al_2O_3 around 12 wt%, FeO between 10 and 20 wt%, TiO_2 between 1 and 2 wt%, MgO around 15wt%, Na_2O around 2–3 wt% and CaO around 10 wt%). Apart from Na_2O and TiO_2 which are enriched in the silicate films (Fig. 6), the composition is relatively close to that of the bulk graphite–garnet pyroxenite (taken from Pearson *et al.*, 1993).

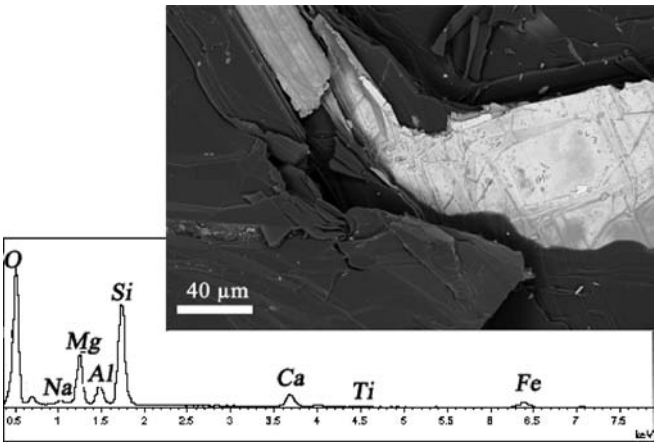

Fig. 4. FE-SEM image (BSE mode on uncoated sample) of a thin film of insulating material (high brightness due to electron accumulation) intercalated between stacks of (001) graphitic planes. The thin film is moulded by the folded graphite planes. The composition of the film is displayed on the EDS spectrum, which shows SiO_2, MgO, Al_2O_3 and CaO as main oxide constituents.

5.3. Isolated globular micro-inclusions

The detailed FE-SEM inspection of the graphite aggregates revealed numerous micro-inclusions of approximately globular shape with sizes between 1 and 10 µm, and a variety of chemical compositions. The inclusions mentioned in this section are only those encountered in more than one specimen of graphite aggregate. They, however, represent a much smaller volume proportion than the silicate films described above. Among them, the most abundant are carbonates, either calcite (as indicated by micro-Raman spectroscopy) or dolomite, with sizes up to 10 µm. Calcium sulphates are also relatively abundant and present in each of the studied graphite aggregate. In addition to carbonates and calcium sulphate(s) [the hydration level could not be determined], some nickel metal (no oxygen on the EDS spectra) and titano-magnetite grains have been found in each of the investigated specimens.

Salt-rich inclusions were not observed in all sections. Where present, they contain potassium and sodium chlorides (and, less commonly, $CaCl_2$). They are sometimes associated with sulphates. Micrometric silica grains and iron sulphides have also been encountered in a few instances.

5.4. Diamond micro-crystals

The powder obtained by grinding a set of four graphite aggregates and used for X-ray diffraction was investigated using FE-SEM. Two submicrometric pseudo-euhedral grains were found to be exclusively composed of carbon as indicated by the energy-dispersive spectra. Their morphology totally differs from that of graphite (Fig. 7a, b) and clearly shows a three-dimensional development, with a pyramidal shape (three-fold crystallographic axis).

Micro-Raman spectra (514.5 nm) collected on these grains are in excellent agreement with a diamond spectrum, with a main band (F2g) centred at around 1332 cm^{-1} and a second at 1582 cm^{-1} (Fig. 7). In order to dismiss the possibility of diamond contamination in the course of the sample preparation (*e.g.,* pollution from the mortar), microdiamonds were searched for *in situ*, in the unground hand-extracted graphite aggregates, by combining FE-SEM, Raman-microspectrometry as well as cathodoluminescence (CL) spectral analysis. The CL spectrum of the micro-diamond displayed on Fig. 7d and characterised beforehand with Raman microspectroscopy was used as a reference to locate further grains. Five other micro-diamond crystals isolated within coarse-grained graphite areas were found by this procedure. They are mostly subhedral to anhedral and their size ranges from 0.5 to 2 µm (Fig. 7c).

A comparative spectroscopy study (micro-Raman and cathodoluminescence) between these natural diamonds and diamonds in the 1-µm polishing materials used in other instances at the Laboratoire de Géologie (ENS, Paris) has been carried out. Diamond grains from paste and sprays are mostly anhedral, although subhedral morphologies are also present.

The Raman band position and full width at half maximum (FWHM), given with a 2σ uncertainty, were measured on both polishing and Beni Bousera diamonds using the 786 nm laser excitation (1200 grooves/mm grating) for different laser powers (given as percentage of 300 mW). Diamonds from paste and spray (2–3 spectra, each the result of three accumulations of 20 s) show, for 0.5 % laser power, a band centred at 1332.6 ± 0.1 cm^{-1} and 1333.41 ± 0.02 cm^{-1}, respectively, with a FWHM of 4.6 ± 0.4 and 3.5 ± 0.2 cm^{-1}, respectively. When the laser power is increased to 10 %, FWHM increases to 6.1 ± 0.1 cm^{-1} (1332.44 ± 0.05 cm^{-1}) for the diamond paste whereas it remains constant (3.49 ± 0.03 cm^{-1}, position $= 1333.39 \pm 0.05$ cm^{-1}) for diamond spray. Diamonds found in the Beni Bousera graphite aggregates (4 spectra) have a different behaviour since their FWHM increases slightly from 0.5 to 10 % laser power (3.5 ± 0.2 to 4.6 ± 0.3 cm^{-1}, respectively) whereas band position shifts from 1333.36 ± 0.03 down to 1330 ± 1 cm^{-1}. The FWHM is also found to vary significantly with the grating. Using 1800 grooves/mm grating (10 % red-laser power), we find FWHM values for the polishing diamonds of 4.5 ± 0.4 cm^{-1} which are lower than those of diamonds recovered in the Beni Bousera graphite aggregates (5.3 ± 0.2 cm^{-1}).

Cathodoluminescence spectra were also recorded, on both diamond types. The CL spectra on polishing diamonds were either collected on individual crystals or by averaging on a large population of grains (over several tens of particles). At first glance, all the recorded spectra (polishing and Beni Bousera) are similar with a main CL emission band around 526 nm along with a second one at 577 nm. The latter band is however narrower for diamonds from the polishing material (Fig. 8). Upon closer inspection, CL spectra of polishing and Beni Bousera diamonds also show marked differences. These differences are mostly found in the 800–1000 nm range where both diamond paste and spray are characterized by two emission bands at 810 and 888 nm of variable

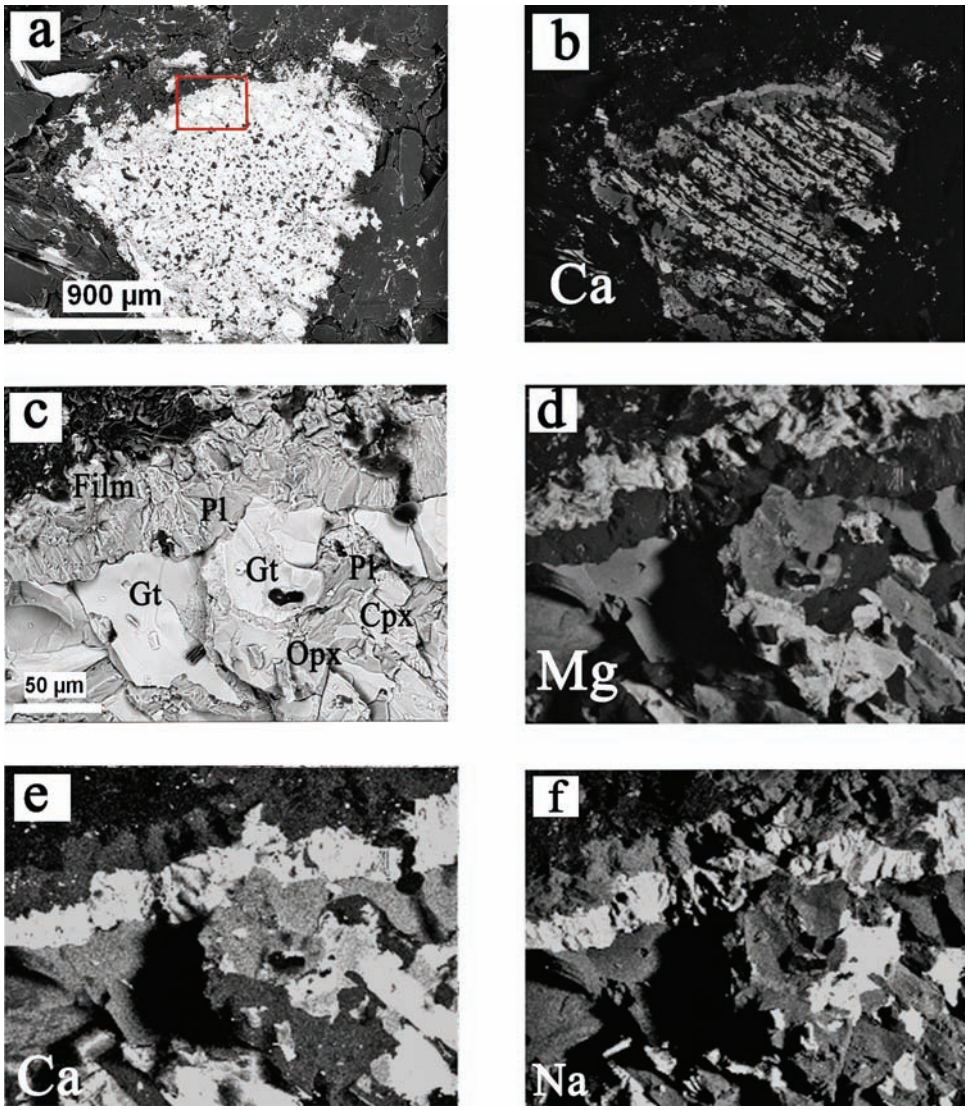

Fig. 5. SEM imaging and elemental X-ray mapping on a macro-inclusion (*ca.* 1 mm across) in the core of a graphite aggregate. (a) BSE image after gold-palladium coating. (b) The Ca$K\alpha_1$ X-ray map outlines the striped texture composed of orthopyroxene lamellae (*dark*) exsolved within a clinopyroxene grain (*white stripes*) as well as a thin plagioclase-rich symplectite rim. (c) Enlargement of the symplectite rim, BSE image (Gt, garnet; Opx, orthopyroxene; Cpx, clinopyroxene; Pl, plagioclase; Film, thin silicate film). The exact location of this zone is indicated on (a). (d) Mg X-ray map emphasizing (*bright*) both Opx and film, whereas the Ca map (e) outlines both Cpx and plagioclase, as does the Na X-ray map (f).

relative intensity. Spectra of Beni Bousera diamonds also display the 888 nm band but as the shoulder of a broader emission band centred around 874 nm. Furthermore, at lower wavelength, all polishing diamonds show a CL band around 490 nm which is absent from Beni Bousera diamonds spectra (Fig. 8).

6. Discussion

6.1. Silicate films formation and significance

The new textural evidence of silicate films wetting the graphite aggregates is therefore entirely consistent with and supportive of geochemical and thermobarometric evidence for partial melting of the graphite–garnet pyroxenite at mid- to lower crustal levels (especially if water and/or CO_2 is involved). Partial melting of the Beni Bousera pyroxenite layers is suggested by their extreme incompatible-element depletion, as well as by the decoupling of parent-daughter and isotopic ratios (Pearson *et al*., 1993; Blichert-Toft *et al*., 1999; Pearson & Nowell, 2004). Based on trace-element compositions of different lithologies, several partial melting events have also been described in the Ronda massif (Garrido & Bodinier, 1999; Lenoir *et al*., 2001). This partial melting is inferred to have occurred at relatively shallow crustal level, in the spinel-pyroxenite field (Van der Wal & Vissers, 1993), during the ascent of the Ronda peridotite body which has been tentatively dated at around 22 Ma (Zindler *et al*., 1983).

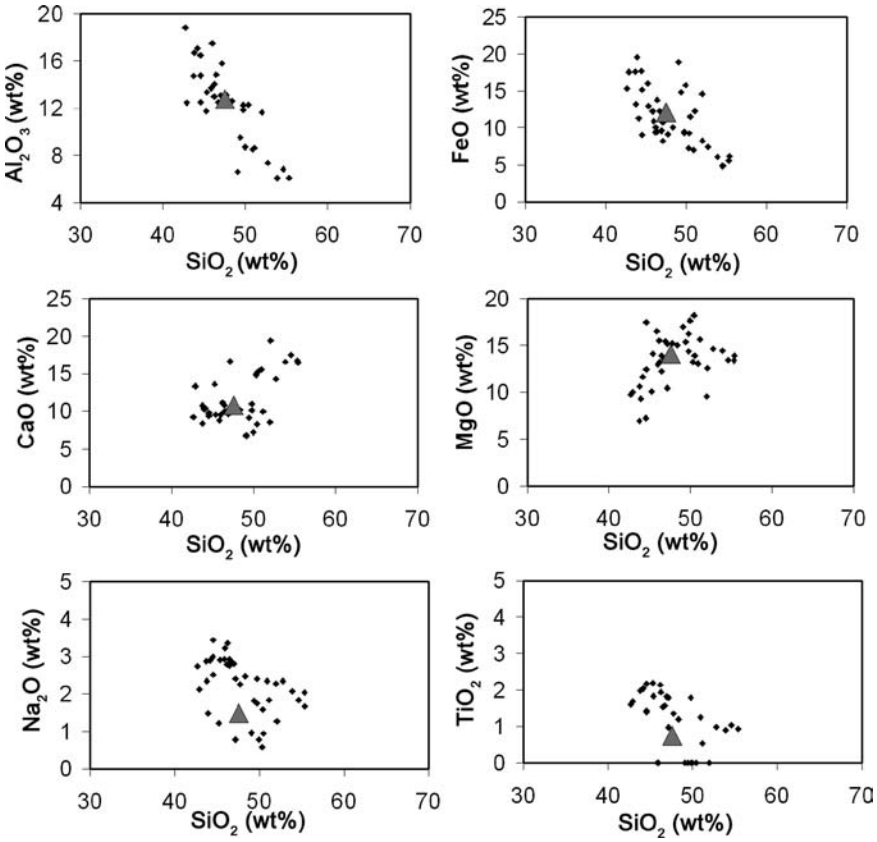

Fig. 6. Semi-quantitative oxide content (EDS) of the silicate films (*dots*) compared to the average bulk composition of the graphitic garnet pyroxenite (*triangle*) after Pearson *et al*. (1993), plotted against SiO_2 content.

The silicate films display a major-element composition (semi-quantitative) which falls close to the average pyroxenite whole-rock composition of Pearson *et al*. (1993). Textural relationships within a graphite aggregate indicate that the film arises from partly retrogressed pyroxene-garnet inclusions, which appear to be the melt source. The widespread distribution of these films all over the graphite aggregate suggests that part of the included films may also originate from melting of the host-rock minerals.

In any event, the thin film morphology indicates a pronounced wetting of the graphite (001) surface by the silicate melt under pressure and temperature. It is worth noting that Laporte *et al*. (2004) used the tendency of partial melts to migrate within micro-cracks formed in graphite containers (Fig. 4b, c in Laporte *et al*., 2004) in order to study their composition at melting degrees as low as 0.2 %.

Van der Wal & Vissers (1993) suggested that temperatures of 1087 ± 69 °C have been achieved in the Ronda massif in the course of its uplift (1.0–1.5 GPa). This temperature is consistent with an earlier determination by Kornprobst (1969) who found temperatures of 1100–1200 °C at pressures around 1.5–2.0 GPa. Recent experimental data on Beni-Bousera pyroxenite samples using graphite container indicate dry solidus temperatures of around 1200–1250 °C at 1–1.5 GPa (Lambart *et al*., 2009).

6.2. Other inclusions

Three main inclusion types in the 1–10 μm size range were identified by FE-SEM inspection of the graphite aggregate surfaces: Ca-Mg carbonates, Ca sulphates and Na-K chlorides. The question is whether these inclusions are formed from material (fluid and/or daughter minerals) that was trapped in the original diamond. Pearson *et al*. (1989, 1995) proposed that the difference in graphite texture between the core and ''coat'' of some aggregates may be inherited from coated diamonds. The fibrous coat of such diamonds is known to host a variety of fluid inclusions, with K-rich chloride solutions bearing Na, Mg, Fe and Ca, which may or may not contain Ca-Mg-Fe carbonates as secondary phase (Guthrie *et al*., 1991; Tomlinson *et al*., 2006; Klein-BenDavid *et al*., 2007, 2010; Weiss *et al*., 2009; Kopylova *et al*., 2010). In the few aggregates examined that had ''coat'' graphite, the tiny globular inclusions are evenly distributed over core and coat. In addition, calcium sulphates are uncommon in natural diamonds, which rather host sulphides (*e.g.*, Harris & Gurney, 1979; Bulanova *et al*., 1998; Palyanov *et al*., 2007). Therefore, the tiny inclusions observed in Beni Bousera graphite aggregates most likely derive from former fluid inclusions, but their origin is unclear. Indeed, they could merely reflect late interaction with crustal fluids.

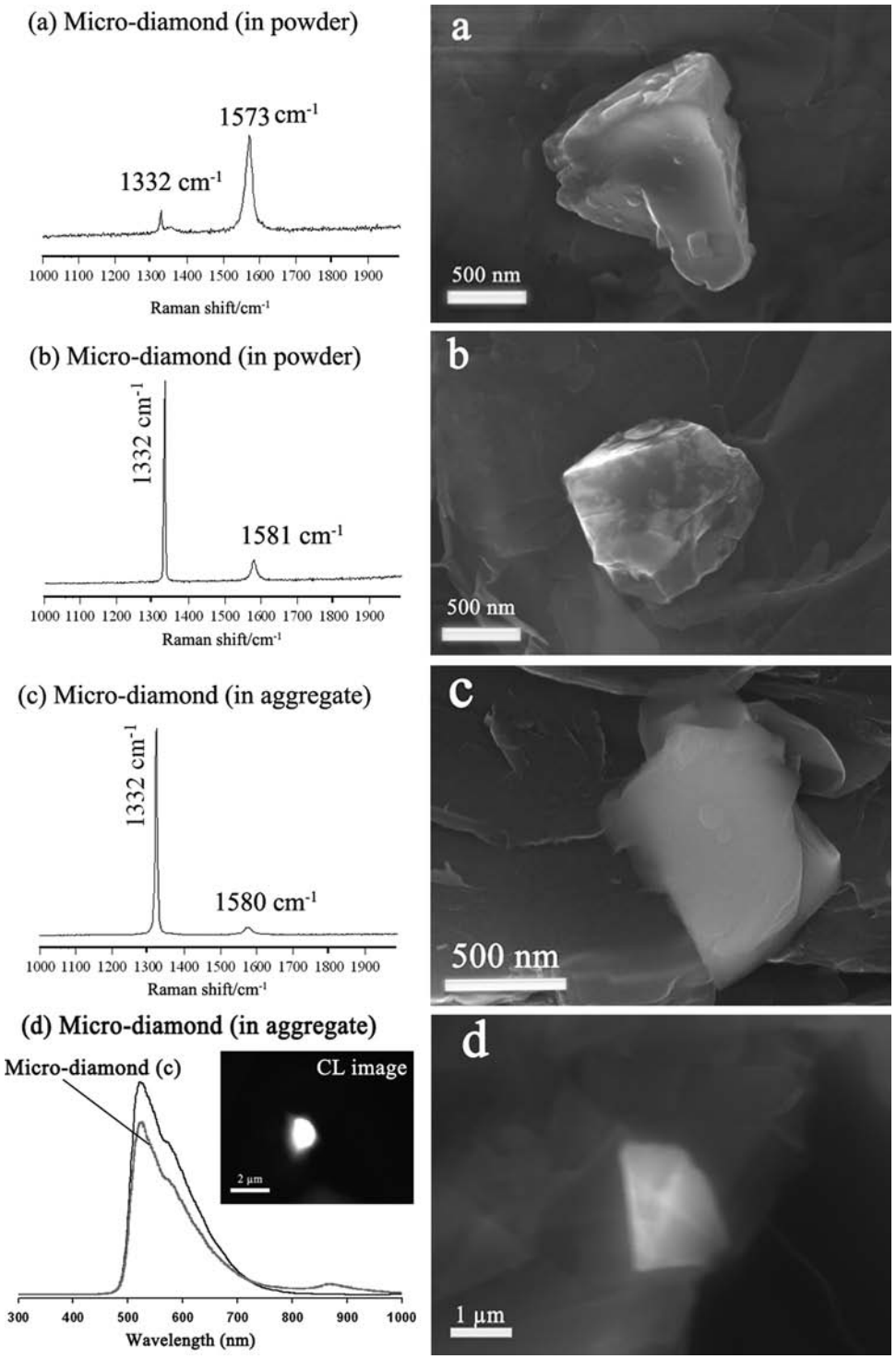

Fig. 7. FE-SEM images (SE in-lens) of diamond micro-crystals and corresponding micro-Raman or cathodoluminescence (CL) spectrum: (a) and (b) from graphite aggregates ground to powder; (c) in freshly broken aggregate, with the preservation of original textural relation between micro-diamond (*bright*) and host graphite aggregate (*dark flakes*); (d) example of diamond grain located using CL with the corresponding CL image and spectrum compared to that of the diamond displayed in (c).

6.3. Micro-diamond: artefact or rock-forming?

The use of diamond as cutting and polishing material is often claimed to be a potential source of contamination in Earth Sciences laboratories. Such diamond-bearing material was purposely avoided in this study but, whenever a new micro-diamond occurrence is reported, especially when it involves a limited number of small grains on a surface, it is fair to ascertain the natural origin using independent criteria. Perraki *et al*. (2009) have proposed a series of criteria

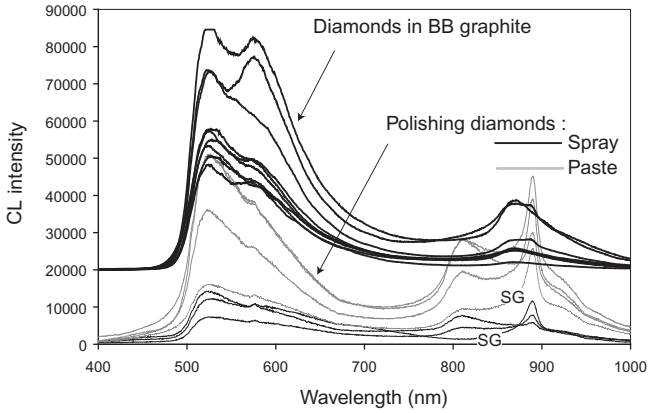

Fig. 8. Comparison between CL emission spectra of a polishing diamond population (spray and paste used at ENS) and diamond inclusions in their graphite host (top spectra), in the 400–1000 nm wavelength range. The spectrum of two polishing diamond single grains is also displayed, noted SG on the Figure.

(morphology, coating, inclusions and Raman characteristics) to distinguish metamorphic micro-diamonds from introduced ones. In the present case, morphology brings no compelling argument, as the subhedral to anhedral diamond shape observed in the graphite aggregates is consistent with the hypothesis of relic diamond within a pseudomorph – and not strikingly different from that in the polishing materials, although the latter mostly show anhedral forms. The small and restricted size (0.5–2 μm) of the diamond crystals observed in graphite is consistent with a contamination origin, but not compelling.

As to Raman characterisation, Perraki *et al*. (2009) showed that the FWHM of the F_{2g} diamond band has a restricted range of values for their polishing materials (2.9–4.3 cm^{-1}) and a significantly wider one, toward higher values, for metamorphic microdiamonds of various provenances (3.0–11 cm^{-1}). Unfortunately, these values being dependent on the operating conditions (as demonstrated here with changing laser excitation power), an absolute inter-laboratory comparison is not sensible.

Are the cathodoluminescence features more diagnostic? At first glance, diamonds in our polishing materials and in the graphite aggregates have similar spectra (Fig. 8). However, marked spectral differences are observed between them: the narrower 577 nm band in the polishing materials, the broad 874 nm band only present in the diamonds found in Beni Bousera graphite aggregates for which, in addition, the low-intensity broad band around 490 nm, found in polishing diamonds, is absent. Groups of emissions in these wavelength ranges have been described for diamonds (Zaitsev, 2001) and related to point defects associated with the presence of nitrogen atoms and the occurrence of atomic vacancies. On the basis of these observations and differences, and of our specific sample-preparation technique, we contend that the diamond observed in graphite is *in situ* and not contamination material (and that CL is an interesting additional tool for such discrimination).

6.4. Micro-diamond formation and preservation: mantle *vs*. metamorphic diamond

The finding of diamond microcrystals within pseudomorphs after diamond may receive a very straightforward interpretation – as relics of former large diamond crystals. However, both the geological setting and the diamond crystal size require careful consideration of diamond formation and preservation. Indeed, in most geodynamic scenarios proposed for both Beni Bousera and Ronda peridotite bodies, the pressure conditions required for diamond formation (*i.e*., >3–3.5 GPa) may have been realized at least twice: in the deep lithospheric mantle (or asthenospheric levels) or later in the high-pressure (H*P*), low-temperature (L*T*) regime of the Alpine subduction. Besides, the micrometre size of the diamond crystals found here is reminiscent of low-temperature metamorphic microdiamond and could suggest a metamorphic rather than upper-mantle origin, *i.e*. late nucleation and growth within the graphite aggregates. In this case, one would be dealing with incipient transformation of graphitic matter into diamond. To our knowledge, such solid-state diamond formation from graphite has been documented only in the case of shock-metamorphism (*e.g*., El Goresy *et al*., 2001) and in experimental studies (*e.g*., Bovenkerk *et al*., 1959; Bundy, 1963; Naka *et al*., 1976; Irifune *et al*., 2004). Le Guillou *et al*. (2006) showed that nano-diamond nucleation kinetics is strongly dependent on both the structure and microtexture of the graphitic precursor, diamond preferentially nucleating on structural defects. Therefore, in such a solid-state hypothesis, microdiamonds nucleating in the graphite aggregates are expected to be preferentially found in the less ordered graphite of the aggregate rims (*cf*. Raman spectroscopy results) – which is not the case.

On the contrary, reports of ascertained ''regional metamorphic'' microdiamonds bring more and more evidence for direct precipitation of microdiamond from complex COH fluids (Stöckhert *et al*., 2001; Dobrzhinetskaya *et al*., 2003; Carswell & van Roermund, 2005; Hwang *et al*., 2005; Vrijmoed *et al*., 2006, 2008). Such an origin may also well be that of most ''kimberlitic'' diamonds, as shown by their inclusions (*e.g*., Stachel & Harris, 2008) and their possible nucleation on graphite flakes that are then preserved as inclusion without evidence of corrosion or resorption (*e.g*., Nasdala *et al*., 2005).

The direct transformation of graphite into diamond in nature, like in the laboratory, might require a very large overstepping of the graphite-diamond equilibrium curve, *i.e*. conditions far inside the diamond stability field. If such conditions are met in shock metamorphism, they might never have been reached by UH*P* metamorphic rocks exhumed in collision zones.

The assumption that the microdiamonds observed here are relics of larger upper-mantle diamonds preserved within graphite aggregates is therefore preferred here. Compelling evidence of partial graphitization of exhumed metamorphic diamonds has already been presented (*e.g*.,

Dobrzhinetskaya *et al*., 2001, 2003; Korsakov *et al*., 2010). In particular, Korsakov *et al*. (2010) reported on residual microdiamonds surrounded by retrograde graphite rosettes, in the Kokchetav UH*P* massif (Kazakhstan). Interestingly, this type of texture suggests that polymorphic diamond retrogression can proceed from surface to core with kinetics that are then surface-area, and consequently, grain-size dependent. This observation is supported by experimental data at 2 GPa which show a significant decrease in diamond–graphite conversion degree as a function of grain sizes in the 5 nm to 35 μm range (Qian *et al*., 2004). The activation energy of the transition seems to increase with grain size (Qian *et al*., 2004), in agreement with the fact that both structure and microtexture of the graphitic product are themselves dependent on the grain size (Qian *et al*., 2001). Therefore, the growth of the graphitic product might be the rate-limiting process. The activation energy of the transformation strongly depends on the diamond faces that are involved (Davies & Evans, 1972). Furthermore, metal inclusions have been shown to act as catalysts for the intracrystalline crystallization of graphitic products (Pantea *et al*., 2002). Finally, fluids such as oxygen (Fedoseev *et al*., 1986) or supercritical water (*e.g.*, Qian *et al*., 2001) have been shown to strongly affect the transformation kinetics. Under these circumstances and without knowing the temperature-time history of the host-rock, a kinetic evaluation of the likelihood of preserving microdiamonds in large retrogressed graphite aggregates (*i.e*., for transformation rates over 99.9 %) is subject to large uncertainties. From a purely kinetic viewpoint, due to the general asymptotic nature of polymorphic transformation extent (ξ) *versus* time (t) curves, either towards high transformation rates (Avrami, 1939) or towards a limited transformation degree (*see* Qian *et al*., 2001, for the diamond–graphite transition, in particular), the transformation rate ($\frac{\partial \xi}{\partial t}$) tends toward zero for the smallest fractions of remaining diamond. This type of behaviour clearly favours the preservation of tiny fractions of original diamond, even for thermochemical conditions under which diamond would be expected to have entirely converted into graphite.

7. Concluding remarks

Graphite aggregates in garnet pyroxenite from Beni Bousera reveal an extremely contrasted geodynamical history involving, successively, deep-seated diamond formation, diamond graphitization in the course of the massif uplift under anomalously high temperatures and, finally, partial melting. Despite the extreme temperature conditions experienced by the graphite–garnet pyroxenite, relics of the original diamonds seem to have survived in the form of micro-diamond included in the large graphite flakes in the core of the aggregates. An alternative, metamorphic origin for these micro-diamonds is unlikely for kinetic and textural reasons. In any event, the micro-diamonds must have survived, within soft graphite aggregates, a temperature event (far) above the blocking temperature of the Sm-Nd isotopic system (garnet–pyroxene, *i.e.*, >800 °C) which took place about 20–25 Ma ago. A thermal event is indeed recorded in the surrounding metamorphic nappes (*e.g.*, Negro *et al*., 2006) which is even the source of anatectic magmatism (Rossetti *et al*., 2010). This event is interpreted as the result of the ascent of the hot upper-mantle units (including the Beni Bousera massif) and appears to be coeval with thinning of the whole lithosphere during an Oligo-Miocene extensional event (Negro *et al*., 2006). The temperature in the Beni Bousera massif itself has actually reached values as high as *ca*. 1100 °C (Kornprobst, 1969; Van der Wal & Vissers, 1993, for the Ronda massif) which led to partial melting of the graphite–garnet pyroxenite (*see* silicate films). Considering these high temperatures, the most striking result of this study lies more in the preservation of diamond relics than in their formation.

Acknowledgements: Nathaniel Findling, Abdeltif Lahfid and Omar Boudouma are warmly thanked for their help at running FE-SEM, micro-Raman and CL devices, respectively. We are grateful to Yves Pinquier for preparing a specific sample holder for the SEM analyses. We would also like to thank Bruno Goffé for having initiated the French–Moroccan collaboration. FE, FB and MB are indebted to CNRS and CNRST for funding the project entitled ''Caractérisation thermobarométrique des granulites et péridotites rifo-bétiques dans la Méditerranée occidentale''). CNRS is also acknowledged for funding FE's PhD work through the BDI – PED programme. We appreciate the thoughtful reviews by Larissa Dobrzhinetskaya and Thomas Stachel, which substantially improved the manuscript.

References

Avrami, M. (1939): Kinetics of phase change. *J. Chem. Phys*., **7**, 1103–1112.

Balasooriya, N.W.B., Touzain, Ph., Bandaranayake, P.W.S.K. (2007): Capacity improvement of mechanically and chemically treated Sri Lanka natural graphite as an anode in Li-ion batteries. *Ionics*, **13**, 305–309.

Blichest-Toft, J., Albarède, F., Kornprobst, J. (1999): Lu-Hf Isotope Systematics of Garnet Pyroxenites from Beni Bousesa, Morocco. Implication for Basalt Origin, *Science*, **283**, 1303–1306.

Bovenkerk, H.P., Bundy, F.P., Hall, H.T., Strong, H.M., Wentorf, R.H., Jr. (1959): Preparation of diamond. *Nature*, **184**, 1094–1098.

Bulanova, G.P., Griffin, W.J., Ryan, C.G. (1998): Nucleation environment of diamonds from Yakutian kimberlites. *Mineral. Mag*., **62**, 409–419.

Bundy, F.P. (1963): Direct conversion of graphite to diamond in static pressure apparatus. *J. Chem. Phys*., **38**, 631–643.

Carswell, D.A. & van Roermund, H.L.M. (2005): On multi-phase mineral inclusions associated with microdiamond formation in

mantle-derived peridotite lens at Bardane on Fjortoft, west Norway. *Eur. J. Mineral*., **17**, 31–42.

Chalouan, A. & Michard, A. (2004): The Alpine Rif Belt (Morocco): a case of mountain building in a subduction-subduction-transform fault triple junction. *Pure Appl. Geophys*., **161**, 489–519.

Davies, G. & Evans, T. (1972): Graphitization of diamond at zero pressure and at a high pressure. *Proc. R. Soc. Lond. A*, **328**, 413–427.

Davies, G.R., Nixon, P.H., Pearson, D.G., Obata, M. (1993): Tectonic implications of graphitized diamonds from the Ronda peridotite massif, southern Spain. *Geology*, **21**, 471–474.

Dobrzhinetskaya, L.F., Green, H.W., II, Mitchell, T.E., Dickerson, R.M. (2001): Metamorphic diamonds: mechanism of growth and inclusion of oxides. *Geology*, **29**, 263–266.

Dobrzhinetskaya, L.F., Green, H.W., Bozhilov, K.N., Mitchell, T.E., Dickerson, R.M. (2003): Crystallization environment of Kazhakstan microdiamond: evidence from nanometric inclusions and mineral associations. *J. Metamorph. Geol*., **21**, 425–437.

El Goresy, A., Gillet, Ph., Chen, M., Künstler, F., Graup, P., Stähle, V. (2001): In situ discovery of shock-induced graphite-diamond phase transition in gneisses from the Ries Crater, Germany. *Am. Mineral*., **86**, 611–621.

Erdosh, G. (1970): Geology of Bogala mine, Ceylon and origin of vein-type graphite. *Miner. Deposita*, **5**, 375–382.

Fedoseev, D.V., Vnukov, S.P., Bukhovets, V.L., Anikin, B.A. (1986): Surface graphitization of diamond at high temperatures. *Surf. Coat. Technol*., **28**, 207–214.

Garrido, C.J. & Bodinier, J.L. (1999): Diversity of mafic rocks in the Ronda peridotite: evidence for pervasive melt-rock reaction during heating of subcontinental lithosphere by upwelling asthenosphere. *J. Petrol*., **40**, 729–754.

Guthrie, G.D., Jr, David, R.V., Navon, O., Rossman, G.R. (1991): Submicrometer fluid inclusions in turbid-diamond coats. *Earth Planet. Sci. Lett*., **105**, 1–12.

Harris, J.W. & Gurney, J.J. (1979): Inclusions in diamond. *in* ''The Properties of Diamond'', J.E. Field, ed., Academic Press, London, 555–591.

Hwang, S.L., Shen, P., Chu, H.T., Yui, T.F., Liou, J.G., Sobolev, N.V., Shatsky, V.S. (2005): Crust-derived potassic fluid in metamorphic microdiamond. *Earth Planet. Sci. Lett*., **231**, 295–306.

Irifune, T., Kurio, A., Sakamoto, S., Inoue, T., Sumiya, H., Funakoshi, K. (2004): Formation of pure polycrystalline diamond by direct conversion of graphite at high pressure and high temperature. *Phys. Earth Planet. Inter*., **143–144**, 593–600.

Jolivet, L., Augier, R., Faccenna, C., Negro, F., Rimmele, G., Agard, P., Robin, C., Rossetti, F., Crespo-Blanc, A. (2008): Subduction, convergence and the mode of backarc extension in the Mediterranean region. *Bull. Soc. Géol. Fr*., **179**, 525–550.

Klein-BenDavid, O., Izraeli, E.S., Hauri, E., Navon, O. (2007): Fluid inclusions in diamonds from the Diavik mine, Canada and the evolution of diamond-forming fluids. *Geochim. Cosmochim. Acta*, **71**, 723–744.

Klein-BenDavid, O., Pearson, D.G., Nowell, G.M., Ottley, C., McNeill, J.C.R., Cartigny, P. (2010): Mixed fluid sources involved in diamond growth constrained by Sr–Nd–Pb–C–N isotopes and trace elements. *Earth Planet. Sci. Lett*., **289**, 123–133.

Kopylova, M., Navon, O., Dubrovinsky, L., Khachatryan, G. (2010): Carbonatitic mineralogy of natural diamond-forming fluids. *Earth Planet. Sci. Lett*., **291**, 126–137.

Kornprobst, J. (1969): Le massif ultrabasique des Beni Bouchera (Rif Interne, Maroc): Etude des péridotites de haute température et de haute pression et des pyroxénolites, à grenat ou sans grenat, qui leur sont associées. *Contrib. Mineral. Petrol*., **23**, 283–322.

Kornprobst, J., Piboule, M., Roden, M., Tabit, A. (1990): Corundum-bearing garnet clinopyroxenites at Beni Bousera (Morocco): original plagioclase-rich gabbros recrystallized at depth within the mantle? *J. Petrol*., **31**, 717–745.

Korsakov, A.V., Perraki, M., Zedgenizov, D.A., Bindi, L., Vandenabeele, P., Suzuki, A., Kagi, H. (2010): Diamond–graphite relationships in ultrahigh-pressure metamorphic rocks from the Kokchetav massif, northern Kazakhstan. *J. Petrol*., **51**, 763–783.

Kumar, N., Reisberg, L., Zindler, A. (1996): A major and trace elements and strontium, neodymium, and osmium isotopic study of a thick pyroxenite layer from the Beni Bousera ultramafic complex of northern Morocco. *Geochim. Cosmochim. Acta*, **60**, 1429–1444.

Lambart, S., Laporte, D., Schiano, P. (2009): An experimental study of focused magma transport and basalt peridotite interactions beneath mid-ocean ridges: implications for the generation of primitive MORB composition. *Contrib. Mineral. Petrol*., **157**, 429–451.

Laporte, D., Toplis, M., Seyler, M., Devidal, J.-L. (2004): A new experimental technique for extracting liquids from peridotite at very low degrees of melting: application to partial melting of depleted peridotite. *Contrib. Mineral. Petrol*., **146**, 463–484.

Le Guillou, C., Brunet, F., Irifune, T., Ohfuji, H., Rouzaud, J.-N. (2006): Nanodiamond nucleation below 2273 K at 15 GPa from carbons with different structural organizations. *Carbon*, **45**, 636–648.

Lenoir, X., Garrido, C.J., Bodinier, J.L., Dautria, J.M., Gervilla, F. (2001): The recrystallization front of the Ronda peridotite: evidence for melting and thermal erosion of subcontinental lithospheric mantle beneath the Alboran Basin. *J. Petrol*., **42**, 141–158.

Loomis, T.P. (1975): Tertiary mantle diapirism, orogeny and plate tectonics east of the Strait of Gibraltar. *Am. J. Sci*., **275**, 1–30.

Mostefaoui, S., Perron, C., Zinner, E., Sagon, G. (2000): Metal-associated carbon in primitive chondrites: structure, isotopic composition, and origin. *Geochim. Cosmochim. Acta*, **64**, 1945–1964.

Naka, S., Horii, K., Takeda, Y., Hanawa, T. (1976): Direct conversion of graphite to diamond under static pressure. *Nature*, **259**, 38–39.

Nasdala, L., Hofmeister, W., Harris, J.W., Glinnemann, J. (2005): Growth zoning and strain patterns inside diamond crystals as revealed by Raman maps. *Am. Mineral*., **90**, 745–748.

Negro, F., Beyssac, O., Goffé, B., Saddiqi, O., Bouybaouene, M.L. (2006): Thermal structure of the Alboran Domain in the Rif (northern Morocco) and the Western Betics (southern Spain). Constraints from Raman spectroscopy of carbonaceous material. *J. Metamorph. Geol*., **24**, 309–327.

Palyanov, Yu.N., Shatsky, V.S., Sokol, A.G., Sobolev, N.V. (2007): The role of mantle ultrapotassic fluids in diamond formation. *Proc. Nat. Acad. Sci. U.S.A*., **104**, 22, 9122–9127.

Pantea, C., Gubicza, J., Ungar, T., Voronin, G.A., Zerda, T.W. (2002): Dislocation density and graphitization of diamond crystals. *Phys. Rev. B*, **66**, 094106.

Pasteris, J.D. (1989): In situ analysis in geological thin sections by Laser Raman microprobe: a cautionary note. *Appl. Spectrosc*., **43**, 567–570.

Pearson, D.G. & Nowell, G.M. (2004): Re–Os and Lu–Hf isotope constraints on the origin and age of pyroxenites from Beni

Bousera peridotite massif: implications for mixed peridotite – pyroxenite mantle sources. *J. Petrol*., **45**, 439–455.

Pearson, D.G., Davies, G.R., Nixon, P.H., Milledge, H.J. (1989): Graphitized diamonds from a peridotite massif in Morocco and implications for anomalous diamond occurrences. *Nature*, **335**, 60–66.

Pearson, D.G., Davies, G.R., Nixon, P.H., Mattey, D.P. (1991): A carbon isotope study of diamond facies pyroxenites and associated rocks from the Beni Bousera peridotite, North Morocco. *J. Petrol*., 175–189.

Pearson, D.G., Davies, G.R., Nixon, P.H. (1993): Geochemical constraints on the petrogenesis of diamond facies pyroxenites from the Beni Bousera peridotite massif, North Morocco. *J. Petrol*., **34**, 125–172.

Pearson, D.G., Daries, G.R., Nixon, P.H. (1995): Orogenic ultramafic rocks of UHP(diamond facies. *in* ''Ultrahigh Pressure Metamorphism,'' R.G. Coleman & X. Wang, eds. F, Cambridge University Press, Cambridge, 456–510.

Perraki, M., Korsakov, A.V., Smith, D.C., Mposkos, E. (2009): Raman spectroscopic and microscopic criteria for the distinction of microdiamonds in ultrahigh-pressure metamorphic rocks from diamond in sample preparation materials. *Am. Mineral*., **94**, 546–556.

Platt, J.P. & Vissers, R.L.M. (1989): Extensional collapse of thickened continental lithosphere: a working hypothesis for the Alboran Sea and Gibraltar Arc. *Geology*, **17**, 540–543.

Platt, J.P., Allerton, S., Kirker, A., Mandeville, C., Mayfield, A., Platzmann, E.S., Rimi, A. (2003a): The ultimate arc: differential displacement, oroclinal bending, and vertical axis rotation in the External Betic-Rif arc. *Tectonics*, **22**, 1017.

Platt, J.P., Argles, T.W., Carter, A., Kelley, S.P., Whitehouse, M.J., Lonergan, N. (2003b): Exhumation of the Ronda peridotite and its crustal envelope: constraints from thermal modelling of a P-T-time array. *J. Geol. Soc. Lond*., **160**, 655–676.

Qian, J., Pantea, C., Voronin, G., Zerda, T.W. (2001): Partial graphitization of diamond crystals under high pressure and high-temperature conditions. *J. Appl. Phys*., **90**, 1632–1637.

Qian, J., Pantea, C., Huang, J., Zerda, T.W., Zhao, Y. (2004): Graphitization of diamond powders of different sizes at high pressure–high temperature. *Carbon*, **42**, 2691–2697.

Reisberg, L., Allegre, C.J., Luck, J.M. (1991): The Re–Os systematics of the Ronda Ultramafic Complex of southern Spain. *Earth Planet. Sci. Lett*., **105**, 196–213.

Rossetti, F., Theye, T., Lucci, F., Bouybaouene, M.L., Dini, A., Gerdes, A., Phillips, D., Cozzupoli, D. (2010): Timing and modes of granite magmatism in the core of the Alboran Domain, Rif chain, northern Morocco: implications for the Alpine evolution of the western Mediterranean. *Tectonics*, **29**, 2017.

Slodkevich, V.V. (1980): Polycrystalline aggregates of octahedral graphite. *Doklady*, **253**, 194–196 [Translated from Doklady Akademii Nauk SSSR, 1980, Vol. 253, No. 3, 697–700].

Stachel, T. & Harris, J.W. (2008): The origin of cratonic diamonds – constraints from mineral inclusions. *Ore Geol. Rev*., **34**, 5–32.

Stöckhert, B., Duyster, J., Trepmann, C., Massonne, H.-J. (2001): Microdiamond daughter crystals precipitated from supercritical COH plus silicate fluids included in garnet, Erzgebirge, Germany. *Geology*, **29**, 391–394.

Tomlinson, E.L., Jones, A.P., Harris, J.W. (2006): Co-existing fluid and silicate inclusions in mantle diamond. *Earth Planet. Sci. Lett*., **250**, 581–595.

Tubia, J.M. & Cuevas, J. (1986): High temperature emplacement of the Los Reales peridotite nappe (Betic Cordillera, Spain). *J. Struct. Geol*., **8**, 473–482.

Van der Wal, D. & Vissers, R.L.M. (1993): Uplift and emplacement of upper mantle rocks in the western Mediterranean. *Geology*, **21**, 1119–1122.

Van Roermund, H.L.M. (2009): Mantle-wedge peridotites from the northernmost ultra-high pressure domain of the Western Gneiss Region, SW Norway. *Eur. J. Mineral*., **22**, 1085–1096.

Vrijmoed, J.C., van Roermund, H.L.M., Davies, G.R. (2006): Evidence for diamond-grade ultra-high pressure metamorphism and fluid interaction in the Svartberget Fe-Ti garnet peridotite-websterite body, Western Gneiss Region, Norway. *Mineral. Petrol*., **88**, 381–405.

Vrijmoed, J.C., Smith, D.C., van Roermund, H.L.M. (2008): Raman confirmation of microdiamond in the Svartberget Fe-Ti type garnet peridotite, Western Gneiss Region, Western Norway. *Terra Nova*, **20**, 295–301.

Weiss, Y., Kessel, R., Griffin, W.L., Kiflawi, I., Klein-BenDavid, O., Bell, D.R., Harris, J.W., Navon, O. (2009): A new model for the evolution of diamond-forming fluids: evidence from microinclusion-bearing diamonds from Kankan, Guinea. *Lithos*, **112**, 660–674.

Zaitsev, A.M. (2001): Optical Properties of Diamond: a Data Handbook. Springer, Berlin.

Zeck, H.E. (1996): Betic-Rif orogeny: subduction of Mesozoic Tethys under E-ward drifting Iberia, slab detachment shortly before 22 Ma, and subsequent uplift and extensional tectonics. *Tectonophysics*, **254**, 1–16.

— (1997): Discussion of 'Structural petrology of the Ronda peridotite, SW Spain: deformation history' by D. van der Wal and R.L.M. Vissers. In: J. Petrol. 37: 23–43. *J. Petrol*., **38**, 529–531.

Zindler, A., Staudigel, H., Hart, S.R., Endres, R., Goldstein, S. (1983): Nd and Sr isotopic study of a mafic layer from Ronda ultramafic complex. *Nature*, **304**, 226–230.

Received 21 September 2010
Modified version received 9 December 2010
Accepted 17 January 2011